Numerical Analysis of Interaction of a High-Voltage Solar Array with Ionospheric Plasma

Hitoshi Kuninaka* and Kyoichi Kuriki†
Institute of Space and Astronautical Science, Komaba, Meguro-ku, Tokyo, Japan

Three-dimensional analysis of the solar array that exposes the surfaces at a relatively high potential and flies in the ionospheric plasma was conducted. For the standard ionospheric conditions, the drain power was calculated at about 0.3% of the solar generated power, which is rather insignificant. On the other hand, the ion forces were found to be enhanced by the large electric potential difference between the solar array and the plasma and must affect significantly the motion of spacecraft with the neutral particle drag.

Nomenclature

c = unit cord vector = $s \times n$
D = characteristic length of solar array
d = thickness of space charge sheath
$\boldsymbol{d}$ = unit vector of ion drag = $-\boldsymbol{u}$
e = charge of electron
$\boldsymbol{F}$ = vector of total ion force
f = normalized charge density
k = Boltzmann constant
l_{ie} = ion-electron mean free path
$\boldsymbol{l}$ = unit vector of ion lift = $\boldsymbol{d} \times \boldsymbol{p}$
M = ion molecular mass
N,n = dimensional and nondimensional particle densities
$\boldsymbol{n}$ = unit normal vector on conductive surface of solar array
P,Q = collision and reflection momenta
$\boldsymbol{p}$ = unit vector of ion side slip
$= \boldsymbol{u} \times \boldsymbol{n} / |\boldsymbol{u} \times \boldsymbol{n}|$ ($\alpha \neq \pm 90$ deg)
$= \boldsymbol{s}$ ($\alpha = \pm 90$ deg)
R = Larmor radius
$\boldsymbol{s}$ = unit span vector from wing root to tip on solar array
T_e,η = dimensional and nondimensional electron temperatures
t,τ = dimensional and nondimensional times
U = satellite velocity
$\boldsymbol{u}$ = unit vector of array orbital velocity
V,Φ = dimensional and nondimensional potentials
v,u = dimensional and nondimensional particle velocities
x,ξ = dimensional and nondimensional variables in space
α, β = angles of attack and side slip (-90 deg $\leq \alpha, \beta \leq 90$ deg)
Δ = mesh size
ϵ = permittivity of vacuum
θ = incident angle measured from normal
λ_D = Debye length
σ = accommodation coefficient
ω = ion plasma frequency
$\nabla, \tilde{\nabla}$ = nablas for dimensional and nondimensional coordinates

Subscripts

A = properties at wing tip of HVSA
e = electron properties
i = ion properties
o = evaluated in uniform flow
n = normal component
t = tangential component
0 = evaluated at condition of $\Phi \to 0$
∞ = evaluated at condition of $\Phi \to \infty$

Superscript

$'$ = drift condition

Introduction

IN association with high-power capability and light-weight structure as featured in the space station, the output voltage of the solar array is required to be high in order to save the mass of power cable as well as to eliminate dc-to-dc converters. However, the high-voltage solar array (HVSA) that exposes the surfaces having large electric potential difference is affected by undesirable interference with the ionospheric plasma when it flies in the low earth orbit (LEO).

The interference of HVSA can be viewed as follows. The space charge sheath is formed around the conductive surface of HVSA at some potential referring to the plasma potential and collects ions and electrons. The charge transfer and momentum exchange between HVSA and the plasma result in both the drain power and the satellite drag, respectively. The coverglasses of the solar cells are eroded by frequent particle collisions so that their erosion or readhesion to themselves may damage the solar generation capability. Moreover, surface discharges may occur so as to release the electric charges in dielectric surfaces. The discharges may destroy the solar cells and cause electromagnetic interference in onboard instruments. A potential distribution in HVSA relative to the ionospheric plasma adjusts itself in order to collect no net plasma current. The electron impinges on HVSA with its thermal velocity, whereas the ion does the same with the satellite orbital velocity. The difference of the current densities between the two species makes the potential in almost all parts of HVSA lower than the plasma potential, and ions are collected in accordance with the drift probe characteristics. The ion collection is essential to the interference of HVSA with the ionospheric plasma.

The drain power was experimentally studied by McCoy and Konradi[1] and analytically by Katz et al.[2] Both research efforts did not take account of the satellite velocity and regarded the solar array as a stationary probe. Knechtel and Pitts[3] conducted an experiment on the ion drag acting on a satellite model that is biased at the same order of voltage as the plasma thermal energy. The present work numerically analyzes the drain power and the ion forces with a three-dimensional model for the large solar array that moves at the orbital speed and has large electric potential difference.[4]

Received Oct. 23, 1987; revision received April 10, 1987.

*Graduate student, Tokyo University.
†Professor. Member AIAA.

Theory

The plasma parameters in LEO at 500 km altitude are summarized in Table 1.[5] In this condition, the electron thermal velocity v_e is larger than the satellite orbital velocity U, whereas the ion thermal velocity v_i is smaller. Ions are, therefore, approximated to impinge on the satellite with U, whereas electrons do so with v_e.

$$v_e \gg U \gg v_i \tag{1}$$

Under the assumption that HVSA has a 10 m span, the characteristic length D is shorter than the ion-electron mean free path l_{ie} and longer than the plasma Debye length λ_D. These conditions satisfy the basic conditions of Langmuir probe theory and permit the particles to be regarded as plasma moving without collision near HVSA.

$$l_{ie} \gg D \gg \lambda_D \tag{2}$$

The maximum array voltage V_A, the ion kinetic energy $\frac{1}{2}MU^2$, and the electron thermal energy kT_e satisfy the following relations:

$$eV_A \gg \tfrac{1}{2}MU^2 \gg kT_e \tag{3}$$

where the voltage V_A applied to HVSA is assumed to be 1 kV at its tip. The Larmor radius R'_i of the ion for the drift velocity is larger than D, whereas those of ion and electron R_i and R_e with respect to the thermal velocities are smaller. Therefore, the geomagnetic field may little affect the ion collection by HVSA in LEO.

$$R'_i > D > R_i \gg R_e \tag{4}$$

As previously stated, the ion characteristics affect strongly the interference of HVSA rather than those of the electron. In this study, the interference of HVSA with the ionospheric plasma is analyzed numerically about the ion collection; namely, almost the entire zone of HVSA with negative potential relative to the plasma when the model of HVSA is assumed to have distributed linear voltage. Analysis is performed under the following assumptions:

1) Ionospheric environment is regarded as plasma.
2) Electrons are in thermal equilibrium.
3) Ions have zero temperature.
4) Plasma particles move without collision.
5) Geomagnetic field is ignored.
6) Upon impinging on HVSA, the ion is neutralized there and reflected in accordance with a law of the rarefied gasdynamics.

Since we have no scattering data on the solar cell cover, the particle reflection is assumed to be described by the momentum accommodation coefficients, as will be realistically defined in a later section.

HVSA is considered a simple rectangular plate that has a conductive surface on one side and an insulated surface on the other for the following reason. In general, the solar cell is mostly covered with glass, and the solar array potential appears only at the interconnects, which is covered with the plasma sheath. Since the sheath thickness is larger than the interval between the interconnects, the solar array is entirely covered with the sheath and electrically behaves as a single conductive plate. These days, another type of solar cell has been developed that has a coverglass coated with a conductive paint.[6] In such a case, the solar array is strictly a conductor because the conductive coverglasses are connected electrically to one side of cell electrodes.

The Poisson's and kinetic equations are used. The first determines space potential distribution, and the others describe motion for ions and electrons.

$$\nabla^2 V = -\frac{e}{\epsilon}(N_i - N_e) \tag{5}$$

$$M\frac{dv}{dt} = -e\nabla V \tag{6}$$

$$N_e = N_o \exp\left(\frac{eV}{kT_e}\right) \tag{7}$$

where N_o is the plasma density in the uniform flow. Equation (7) is derived from the electron kinetic equation under the assumptions of being isothermal and without mass. Ion density N_i is determined by ion trajectories, and electron density N_e by Boltzmann distribution dependent on the local potential. The aforementioned equations are normalized to the following:

$$\Phi = \frac{-eV}{\frac{1}{2}MU^2}, \quad \eta = \frac{kT_e}{\frac{1}{2}MU^2}, \quad \xi = \frac{x}{U/\omega}, \quad \tau = \omega t$$

$$n_i = \frac{N_i}{N_o}, \quad n_e = \frac{N_e}{N_o}, \quad u = \frac{v}{U}, \quad \omega = \sqrt{\frac{N_o e^2}{\epsilon M}}$$

Normalization by U is characteristic of the present work, whereas the conventional probe theories have used T_e. Equations (5), (6), and (7) are converted as follows:

$$\tilde{\nabla}^2 \Phi = 2f \tag{8}$$

$$f = n_i - n_e \tag{9}$$

$$\frac{du}{d\tau} = \tfrac{1}{2}\tilde{\nabla}\Phi \tag{10}$$

$$n_e = \exp\left(-\frac{\Phi}{\eta}\right) \tag{11}$$

When Φ is small, f is independent only on n_e. On the other hand, with an increase of Φ, the f becomes dependent only on n_i. They are reduced to

$$f_0 = \frac{\Phi}{\eta} \quad (\Phi < 1) \tag{12}$$

$$f_\infty = \eta_i \quad (\Phi \gg 1) \tag{13}$$

Table 1 Plasma parameters in LEO at 500 km altitude

Plasma density, 5×10^5 cm^{-3}	Ionization rate, 0.1	Mean free path of neutral particles, 60 km	Mean free path of ions and electrons, 400 m	Debye length, 0.5 cm	Satellite velocity, 7.6 km/s
	Temperature	Average molecular weight	Thermal velocity	Larmor radius	
Electron	0.2 eV	—	250 km/s	3 cm	
Ion	0.1 eV	20	1.4 km/s	7 m	

Although Eq (12) is not always accurate in the wake, the calculated regions are dominated by large negative potential and the error introduced by this approximation is small. Combining Eqs. (12) and (13), we can construct a single analytical formula as follows:

$$f = 1/(f_0^{-1} + f_\infty^{-1}) \tag{14}$$

Finally, it is needed to solve Eqs. (8), (10), and (14). The details of the calculation scheme will be described in the next section.

Numerical Simulation

Equation (8) is solved by the finite-difference method.[7] Each ion is tracked by solving Eq. (10) on the updated space potential distribution until traveling out of the calculated region or colliding with HVSA. The result gives the ion density distribution, the ion collison distribution on HVSA, and the ion forces. The ion density distribution is inserted in Eq. (14) in order to modify the space potential distribution. These iterations are performed until a self-consistent solution is obtained.

With the selection of a mesh size Δ larger than the nondimensional Debye length $\sqrt{\eta}/2$, difficulty arises in solving Eq. (8), whereas such a choice is efficient for the calculation procedure because the interesting ion sheath is much longer than the Debye length. According to Δ, Eq. (12) is modified into

$$f_0 = \frac{3\Phi}{\Delta^2} \quad (\Phi < 1) \tag{15}$$

where the calculated region is divided by the equal mesh size. This modification leads to an accurate solution as long as the conditions of Eqs. (2) and (3) are kept. The boundary conditions are as follows. On the outer boundary of the calculated region, Φ is equal to zero. On the conductive surface of HVSA, Φ is assumed to be given by the array potential. On the insulator, its gradient $\partial\Phi/\partial\xi_\perp$ perpendicular to the surface is assumed to be zero.

For the purpose of calculation, the ion forces are classified to three components: scattering, ram, and reflection. The scattering is defined as the component due to the momentum exchange between HVSA and the ion particle by electrostatic force without collision. The ram component is referred to the ions impinging on HVSA until infinity. The reflection is defined as the component under the collision, when ions are neutralized on HVSA under the assumptions and no longer influenced by the space electric potential. The difference between the incoming and outgoing ion momenta through the boundaries of the calculated region represents the sum of the scattering and ram components. The reflection component is calculated on HVSA in terms of the accommodation coefficients that are convenient for understanding momentum transfer to a body in free molecule flow. There are two momentum accommodation coefficients, σ_n and σ_t, for the normal and the tangential components of momentum, respectively,

$$\sigma_n = (P_n - Q_n)/P_n$$
$$\sigma_t = (P_t - Q_t)/P_t \tag{16}$$

with P and Q shown in Fig. 1. In the present work, σ_n and σ_t are assumed to be, like in Ref. 8, as follows:

$$\sigma_n = 0.7 \times \cos\theta$$
$$\sigma_t = 0.6 \tag{17}$$

Before starting the numerical simulation, our iteration scheme was verified by applying the Child-Langmuir law in the region where ion flow was regarded as one-dimensional. The numerical and analytical solutions were found to be in good agreement.

The model solar array has a 10 m span, 3 m chord length, and zero thickness and is assumed to be conductive on one side, while insulated on the other side. The spanwise potential distribution is assumed to be linear with a minimum voltage of -1 kV ($\Phi_A = 167$) at the wing tip and 0 V at the wing root. The chordwise potential distribution is constant. Typically, the calculated region is divided into $59 \times 27 \times 31$ uniformly by the constant mesh size. About 40,000 particles are used in order to obtain ion trajectories. The angles of attack and side slip referring to the ion flow are shown in Fig. 2. The drag, side slip, and lift may also be observed there. cies. Therefore, the carrier must be individually recovered from each output signal. Also, symbol timings for the respective data signals are usually independent of each other. Fur-

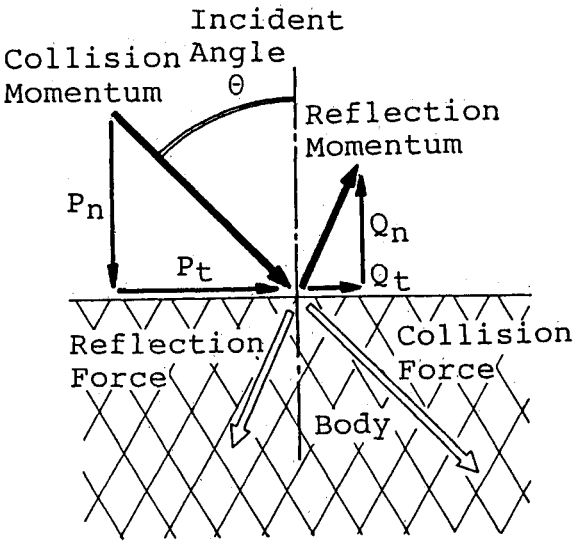

Fig. 1 Geometry and notation of particle collision with surface.

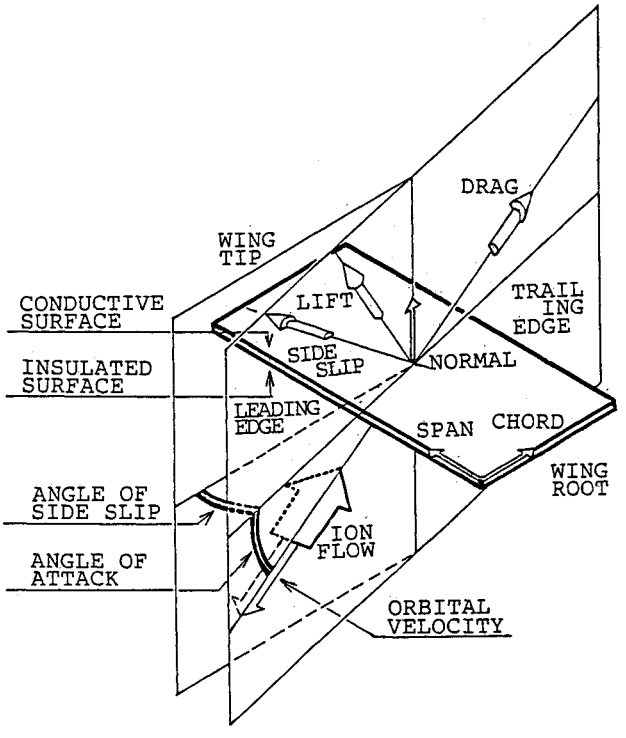

Fig. 2 Coordinates system of solar array and ion flow.

They are defined mathematically as follows:

$$\sin\alpha = -(u,n)$$

$$\text{drag} = (F,d)$$

$$\text{side slip} = (F,p)$$

$$\sin\beta = -(p,c)$$

$$\text{lift} = (F,l)$$

β, however, is not determined at $\alpha = \pm 90$. The position on HVSA is indicated by the spanwise and chordwise locations in the percentage of respective array dimensions.

Results and Discussion

Figure 3 presents both the space potential distributions and the ion trajectories for $\alpha = 0$ and $\beta = 0$, which are shown with plane, front, and side elevations. Figure 4 depicts side elevations at $\alpha = 30$ and $\alpha = -30$ for $\beta = 0$. The results represent accurately the ion sheath and the other data because the space potential converges to zero sufficiently enough in the calculated region. The calculation scheme cannot precisely describe the structure of the wake behind the ion sheath since the electron thermal energy assumes the leading role there. It can be seen that the sheath grows around the high-potential array edge, extends toward the insulated surface, and thickens in the wake side of HVSA because of dilute plasma.

The ion current distribution on the conductive surface of HVSA is shown in Fig. 5, where the contour levels are normalized by the ion current density 0.61 mA/m^2 collected by the unbiased ram surface. The leading edge, wing tip, and corners biased deeply negative collect a considerable sum of the current. The surface area with high current density may be degraded because the ions are accelerated by the array potential and collide with the corresponding kinetic energy. This leads us to select materials resistant to sputtering in the development of the solar cells.

The total ion current, drain power, ion drag, and lift are plotted against the angle of attack at $\beta = 0$ in Figs. 6 and 7. The drain power is expressed by the fraction of the standard solar power generation 4.8 kW that the solar cell of 12% efficiency produces for a 30 m^2 solar array. The ion current is normalized by the ion flux 18 mA on unbiased ram surface having the same area as HVSA. The ion drag and lift are expressed with reference to the neutral particle force 2.9×10^{-5} N on the ram side under the assumption of the same number density as the ion and $\sigma_n = 1$. The ion current and drain power show a similar functional dependence on the angle of attack and assume a maximum value at $\alpha = -90$ where the conductive surface of HVSA confronts the ram direction. The maximum drain power is about 0.3% of the generated power and is regarded as insignificant. The side-slip force by ion is less than the others. The ion lift always has a negative value that represents the ion force traversing from the conductive to the insulated surface. In the neighborhood of $\alpha = 30$, the ion drag shows a negative sign. This means that the thrust is generated by the force due to particle reflection. The ion particles with zero initial velocity, when viewed from the coordinate system fixed to the ionosphere, are accelerated by the array potential and leave backward of HVSA with much reflection velocity losing electric charge after the collision. In other words, HVSA behaves like an ion engine using ionospheric plasma as a propellant. The ion forces are enhanced by the HVSA potential and affect the HVSA motion considerably. It may be possible to control actively the satellite attitude and altitude by the ion forces.

Figure 8 shows the functional dependences of the ion currents on the minimum array voltage $V_A(\Phi_A)$ at the wing tip for the cases of both $\alpha = 0$, $\beta = 0$ and $\alpha = -90$. The array is

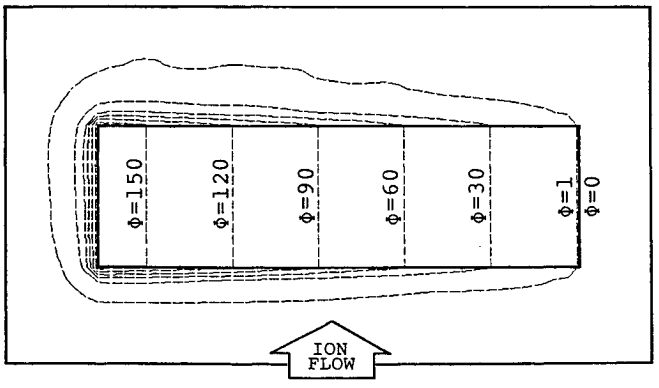

a) Plane elevation

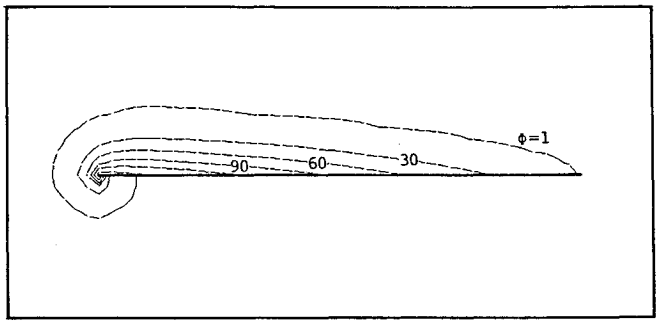

b) Front elevation, at 50% chordwise position

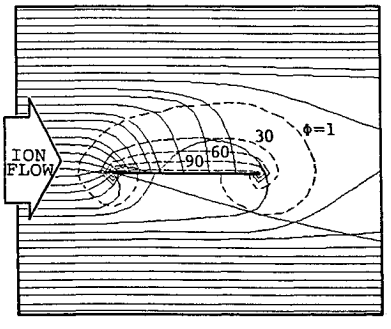

c) Side elevation, at 80% spanwise position

Fig. 3 Space potential contours and ion trajectories around solar array at $\alpha = 0$ and $\beta = 0$. The bold straight lines, broken and solid curves represent solar array, equipotential contour lines, and ion trajectories, respectively. The interval of the equipotential contour lines is about 30 of normalized potential. a) Plane elevation. b) Front elevation at 50% chordwise position. c) Side elevation at 80% spanwise position.

assumed to have the same features as the preceding case except for minimum voltage at the wing tip. In the case of the unbiased array, the nondimensional ion current is equal to one for $\alpha = -90$, whereas it equals zero for $\alpha = 0$ and $\beta = 0$ due to the differences of the virtual areas of HVSA for the ion flow direction. The increment of Φ_A thickens the ion sheath covering HVSA so that both curves of ion currents converge gradually since the ions are collected through the virtual surface area of the ion sheath instead of HVSA. For the case of $\alpha = 0$ and $\beta = 0$, the ion current is approximately proportional to the 0.5 power of the array voltage. This is qualitatively explained as follows. The Child-Langmuir law indicates $d \propto V^{3/4}$ because the ion current density is regarded

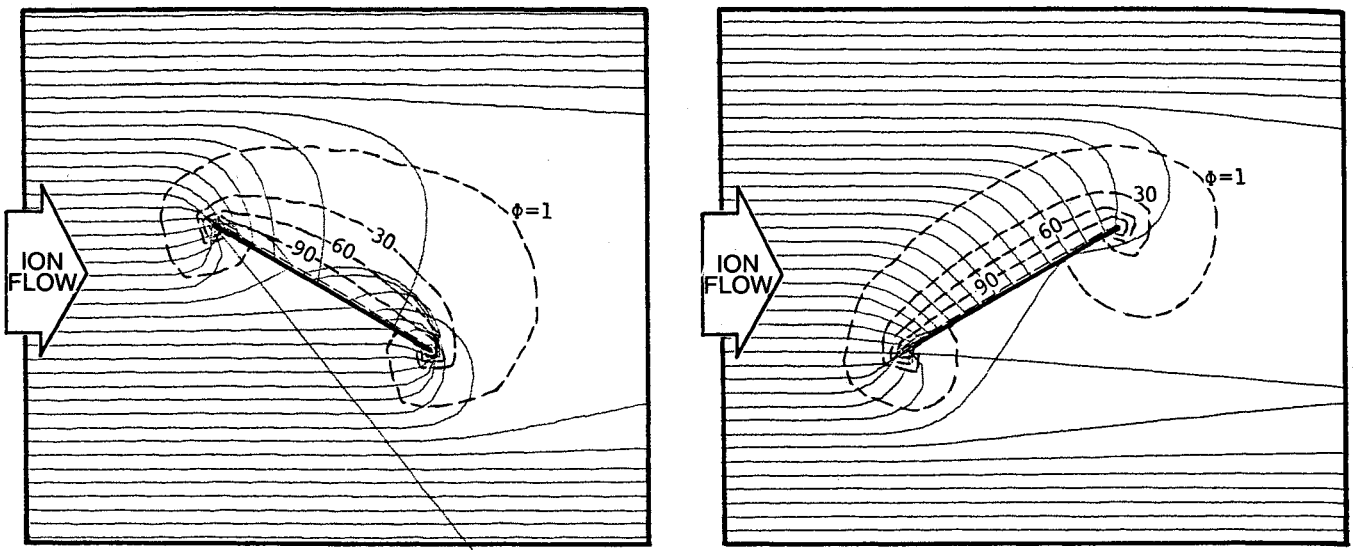

a) $\alpha = 30$ b) $\alpha = -30$

Fig. 4 Side elevations of space potential contours and ion trajectories at 80% spanwise position. The bold straight lines, broken and solid curves represent solar array, equipotential contour lines, and ion trajectories, respectively. The interval of the equipotential contour lines is about 30 of normalized potential.

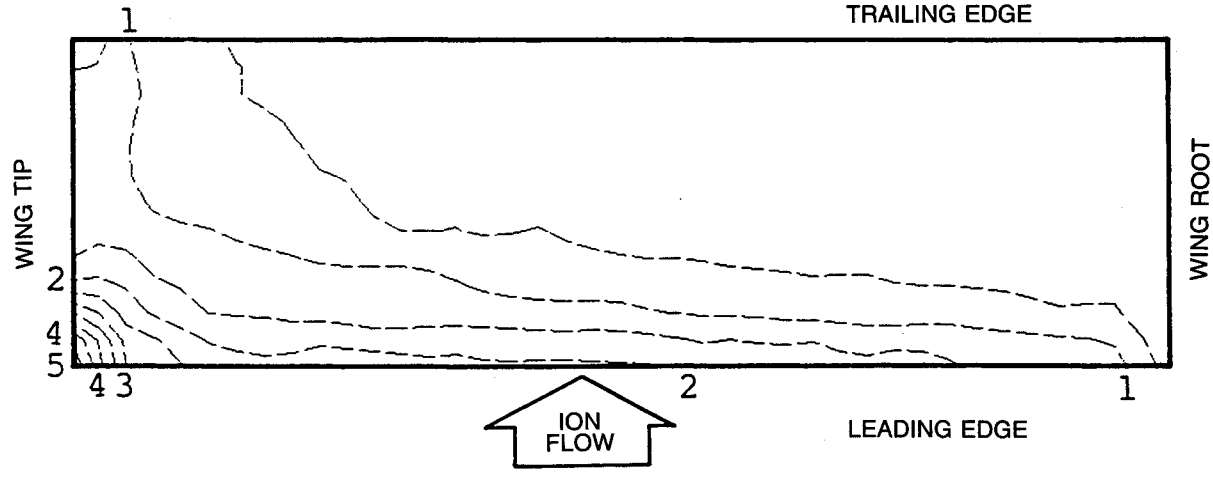

Fig. 5 Distribution of ion current density on conductive surface of solar array at $\alpha = 0$ and $\beta = 0$. The contour levels are expressed in terms of the fraction of the ion current density on the unbiased ram surface.

as constant in LEO. The virtual surface area of the ion sheath is considered proportional to the first power of d owing to $d<D$ in the conditions of this study. Finally, the voltage dependence of the calculated ion current closely represents the 0.75 power law of Child-Langmuir, although the deviation occurs because of three-dimensional effects.

Figure 9 shows characteristics of the ion drag with its components against the array potential $V_A(\Phi_A)$ for the case of $\alpha = -90$. In this case, three components produce the positive drags dominating the lifts and the side slips. The scattering component is far less than the others. Figures 3 and 4 also support this since there are few ions that deviate from their straight courses without colliding with HVSA. Above $\Phi_A = 40$, the reflection component overwhelms the others and induces mostly the ion drag in this case. At the higher Φ_A, the imperfection of the ion neutralization on HVSA may make the real characteristics deviate from the calculation results.

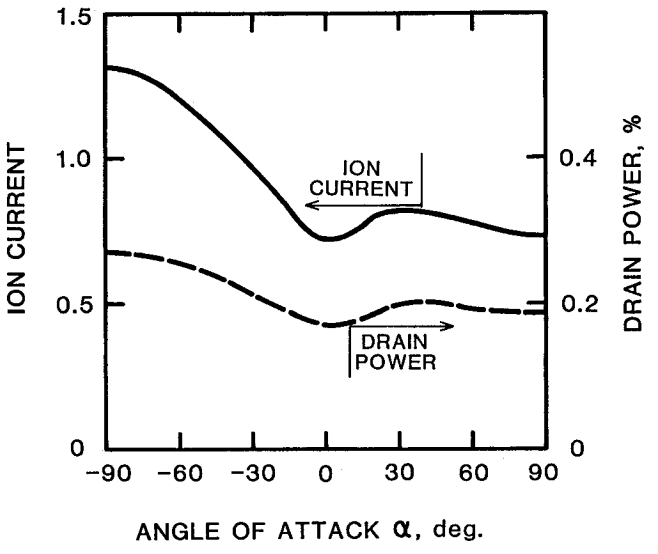

Fig. 6 Dependence of total ion current and drain power on angle of attack at $\beta = 0$. The ion current is normalized by the ion current on the unbiased ram surface. The drain power is expressed by the fraction of the standard solar generation.

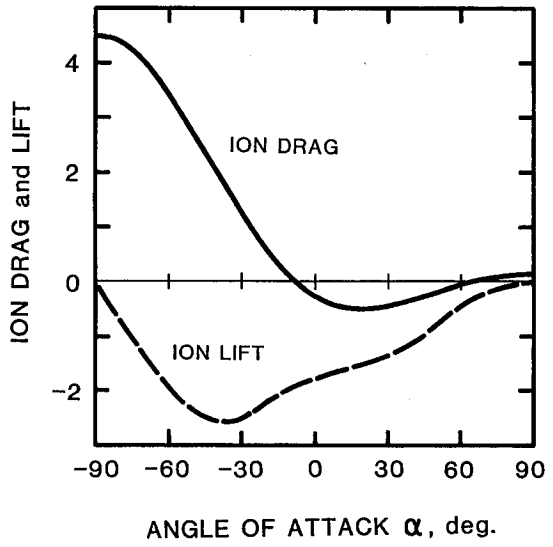

Fig. 7 Dependence of ion drag and lift on angle of attack at $\beta = 0$. Both are normalized by the drag of a neutral particle with the same density as the ion density and $\sigma_n = 1$ on the ram side assumed.

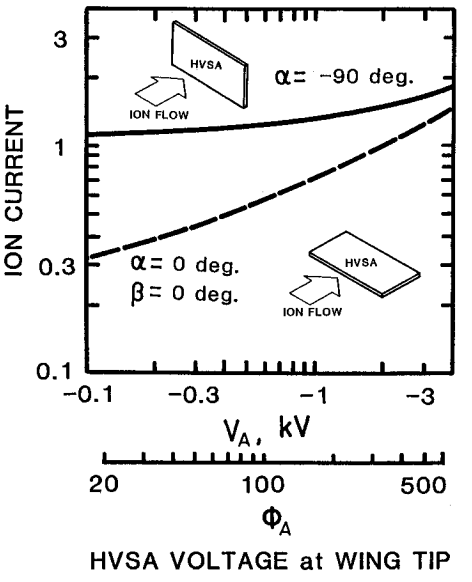

Fig. 8 Dependence of total ion currents on array voltage. They are normalized by the ion current on the unbiased ram surface.

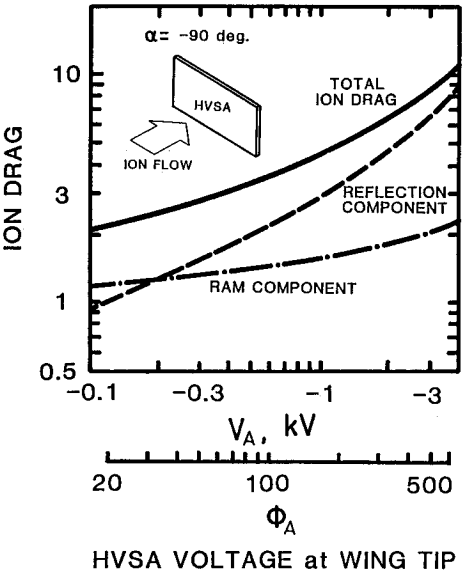

Fig. 9 Dependence of ion drag with components on array voltage. It is normalized by the drag of a neutral particle with the same density as the ion density and $\sigma_n = 1$ on the ram side assumed.

Concluding Remarks

The following were the new findings in the authors' study of HVSA. The sheath grows on both the conductive and insulated wake sides. The ion current distribution on HVSA is strongly dependent on the array voltage and configuration. The drain power amounts to about 0.3% of the generated solar power. The ion forces, which are dominantly induced by the surface reflection, considerably affect the satellite motion with the neutral gas forces. The ionic forces can be applied for the attitude and altitude controls of the spacecraft in LEO.

References

[1]McCoy, J.E. and Konradi, A., "Sheath Effects Observed on a 10 Meter High Voltage Panel in Simulated Low Earth Orbit Plasma," NASA CP-2071, 1978.

[2]Katz, I., Mandell, M.J., Schnuelle, G.W., Parks, D.E., and Steen, P.G., "Plasma Collection by High-Voltage Spacecraft at Low Earth Orbit," *Journal of Spacecraft and Rockets,* Vol. 18, Jan.-Feb. 1981.

[3]Knechtel, D.E. and Pitts, W.C., "Experimental Investigation of Electric Drag on Satellites," *AIAA Journal,* Vol. 2, June 1964.

[4]Kuninaka, H. and Kuriki, K., "Two-Dimensional Analysis of High Voltage Solar Array Interfering with Ionospheric Plasma," *Proceedings of the Symposium on Mechanics for Space Flight Dynamics 1985,* Institute of Space and Astronautical Science Rept. SP-4, 1985.

[5]Al'pert, Y.L., et al., "Space Physics with Artificial Satellites," Consultants Bureau, New York, 1965.

[6]Ijichi, K., et al., "High Voltage Solar Array for MPD Propulsion System," AIAA Paper 85-2047, Sept. 1985.

[7]Roache, P.J., *Computational Fluid Dynamics,* Hermora Publishers, 1976.

[8]Savage, H.F. and Bader, M., "Momentum Accommodation of N^+, N_2^+, and A^+ Incident on Copper and Aluminum from 0.5 to 4 keV," NASA TN D-1976, 1963.